Electronic Supporting Information

Table S1 Selected bond angles (°) for **1**·HCl·H_2O

O1-P1-O2	111.33(12)	O1-P1-C10	109.80(13)
O1-P1-O3	114.70(12)	O2-P1-C10	108.24(12)
O2-P1-O3	104.72(11)	O3-P1-C10	107.74(12)

Table S2 Selected bond angles (°) for **1**·H_2O

O1-P1-O2	114.35(18)	O1-P1-C10	108.56(17)
O1-P1-O3	109.88(16)	O2-P1-C10	109.62(18)
O2-P1-O3	109.32(16)	O3-P1-C10	104.67(17)

Table S3 Selected bond angles (°) for **2**

N1-Zn1-O4	76.23(14)	O1W-Zn1-O2A	92.30(14)
N1-Zn1-O1W	93.58(15)	O1B-Zn1-O2A	118.19(13)
O4-Zn1-O1W	169.81(13)	C1-N1-Zn1	124.1(3)
N1-Zn1-O1B	129.50(14)	C8-O4-Zn1	112.5(3)
N1-Zn1-O2A	111.08(14)	C9-N1-Zn1	115.6(3)
O4-Zn1-O1B	91.85(13)	P1-O1-Zn1B	128.8(2)
O4-Zn1-O2A	91.29(13)	P1-O2-Zn1C	130.64(18)
O1W-Zn1-O1B	94.84(14)		

Symmetry codes: A : x, -y + 1/2, z + 1/2; B: -x + 1, -y, -z + 1; C: x, -y + 1/2, z - 1/2.

Table S4 Selected bond angles (°) for **3**

O1A-Cu1-O2B	93.75(10)	N1-Cu1-O4	75.51(10)
O1A-Cu1-O5C	86.35(10)	P1-O1-Cu1D	137.69(15)
O2B-Cu1-O5C	176.75(10)	P1-O2-Cu1B	133.43(15)
O1A-Cu1-N1	169.70(11)	C8-O4-Cu1	109.09(18)
O2B-Cu1-N1	93.92(10)	C11-O4-Cu1	118.83(18)
O5C-Cu1-N1	86.38(10)	C12-O5-Cu1E	106.4(2)
O1A-Cu1-O4	97.38(9)	C1-N1-Cu1	121.9(2)
O2B-Cu1-O4	91.84(9)	C9-N1-Cu1	117.9(2)
O5C-Cu1-O4	91.36(9)		

Symmetry codes: A: x - 1, y, z; B, -x, -y + 1, -z + 1; C, x, -y + 1/2, z + 1/2; D, x + 1, y, z; E, x, -y + 1/2, z - 1/2.

Table S5 Selected bond angles (^{o}) for **4**

O2A-Fe1-O1B	99.39(15)	N1-Fe1-O4	71.98(12)
O2A-Fe1-O1B	99.39(15)	N1-Fe1-O4	71.98(12)
O2A-Fe1-O5	102.44(15)	P1-O1-Fe1B	151.0(2)
O1B-Fe1-O5	106.71(16)	P1-O2-Fe1C	138.3(2)
O2A –Fe1-N1	112.58(13)	C8-O4-Fe1	119.1(3)
O1B-Fe1-N1	90.39(15)	C11-O4-Fe1	118.3(2)
O5-Fe1-N1	137.85(14)	C12-O5-Fe1	122.8(3)
O2A –Fe1-O4	114.59(14)	C1-N1-Fe1	122.7(3)
O1B-Fe1-O4	145.54(14)	C9-N1-Fe1	118.6(3)

Symmetry codes: A : -x + 2, y + 1/2, -z + 3/2 ; B: -x + 2, -y + 1, -z + 1; C: -x + 2, y - 1/2, -z + 3/2

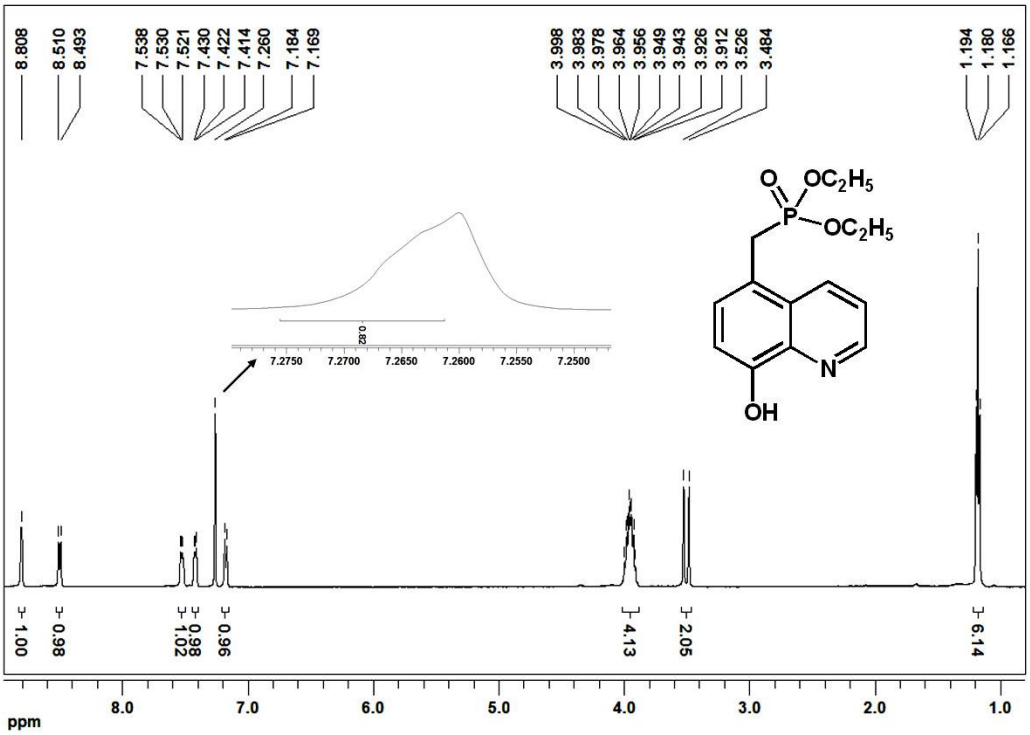

Fig. S1 ^{1}H NMR spectrum of 5dpm8hqH (500 MHz, $CDCl_3$).

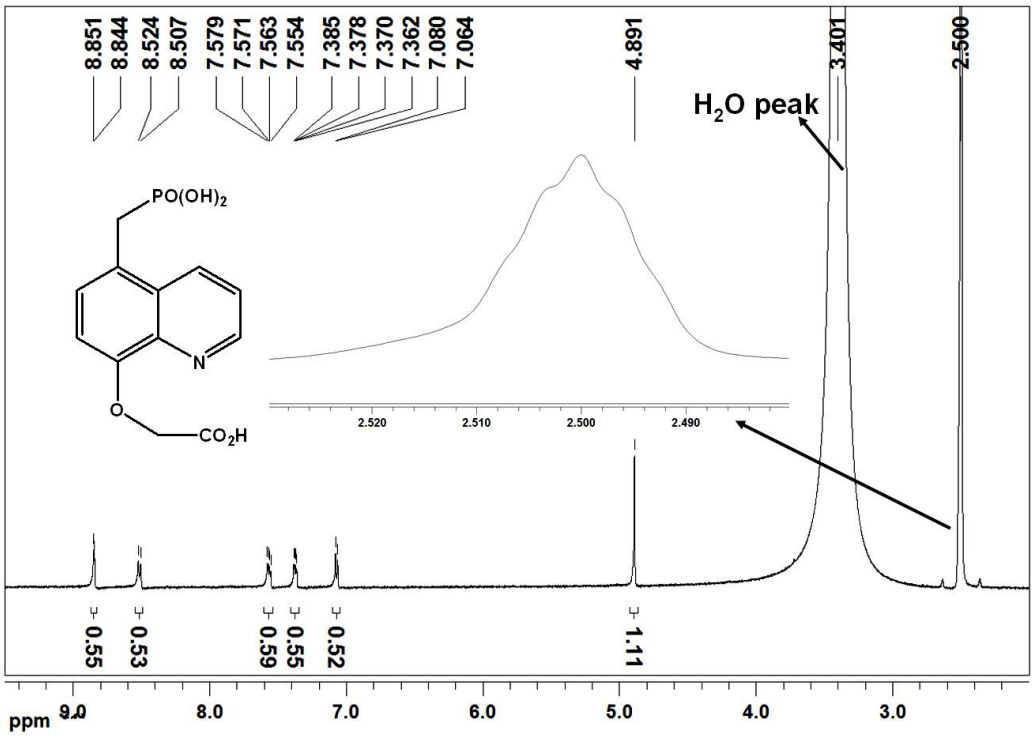

Fig. S2 ^{1}H NMR spectrum of 5pm8cmoqH_3 (500 MHz, DMSO-d_6).

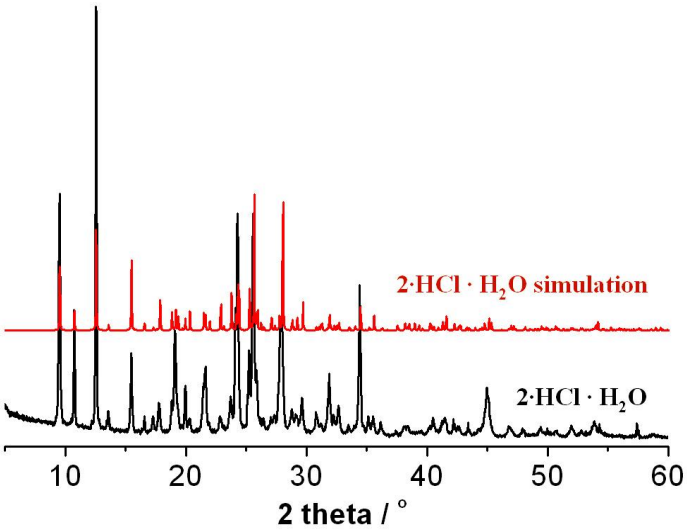

Fig. S3 Experimental and simulated XRD patterns of **1**·HCl·H_2O.

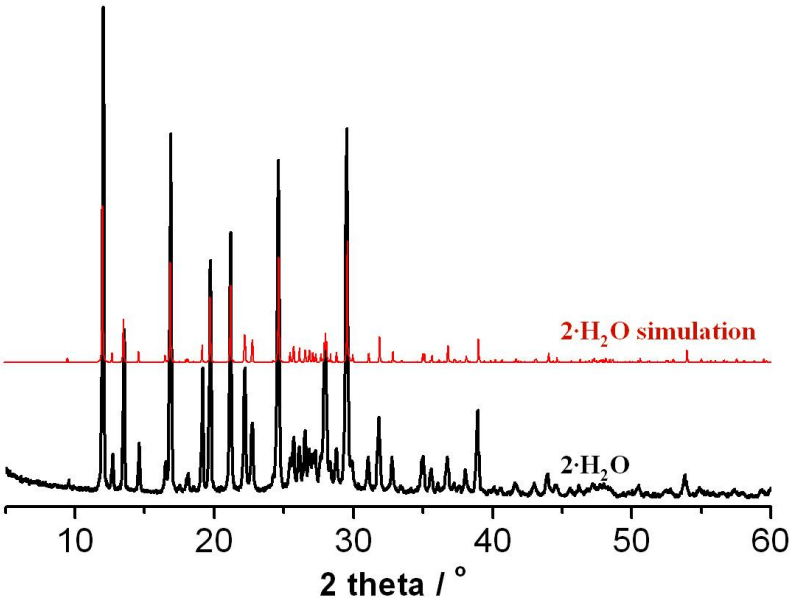

Fig. S4 Experimental and simulated XRD patterns of **1**·H_2O.

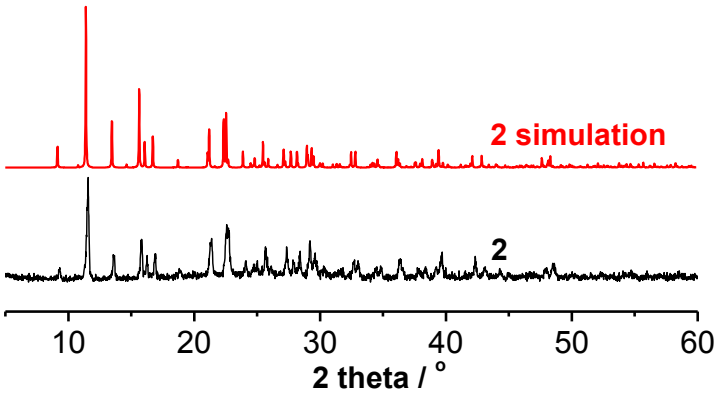

Fig. S5 Experimental and simulated XRD patterns of **2**.

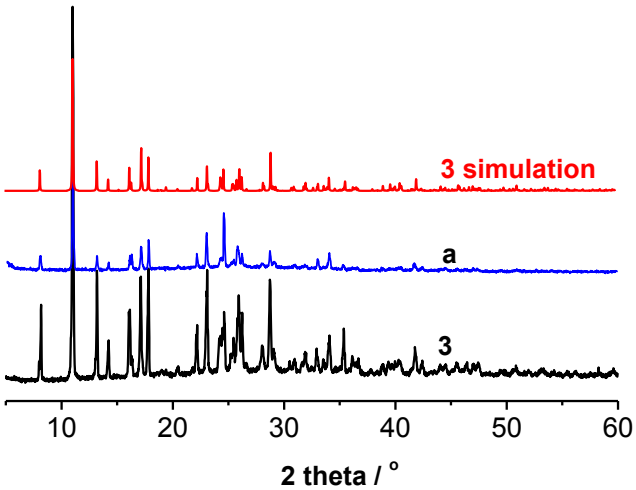

Fig. S6 Experimental and simulated XRD patterns of **3**, and pattern for the rehydration sample of **3-de** (curve a).

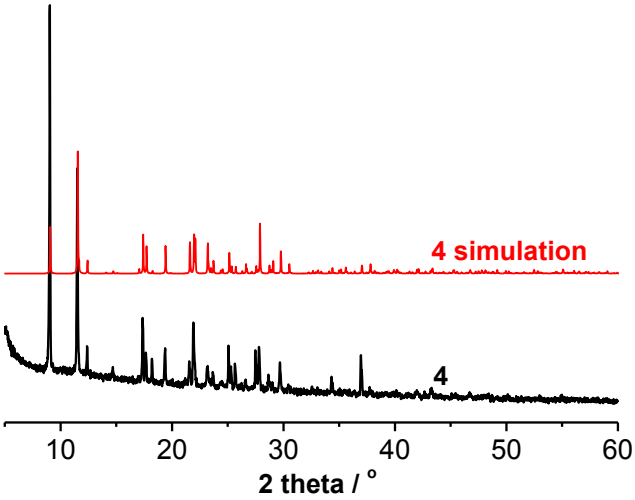

Fig. S7 Experimental and simulated XRD patterns of **4**.

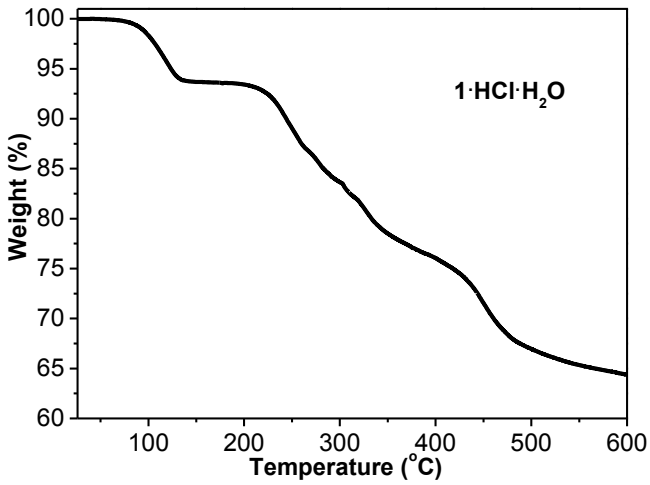

Fig. S8 TG curve of compound **1**·HCl·H_2O.

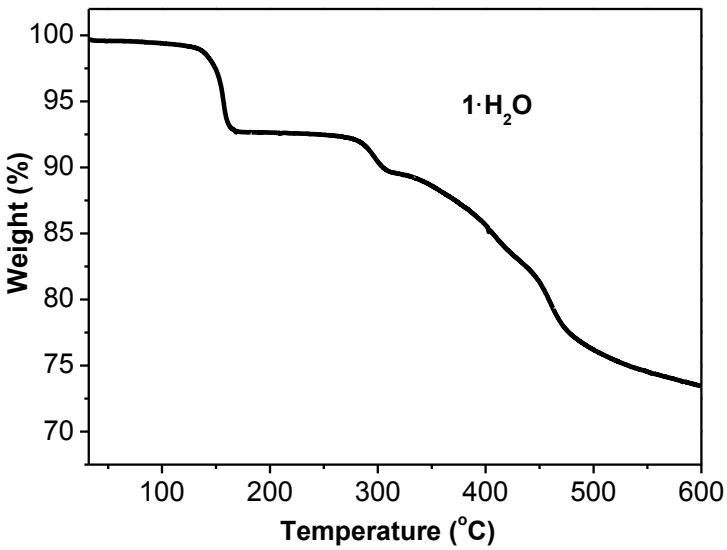

Fig. S9 TG curve of compound **1**·H_2O.

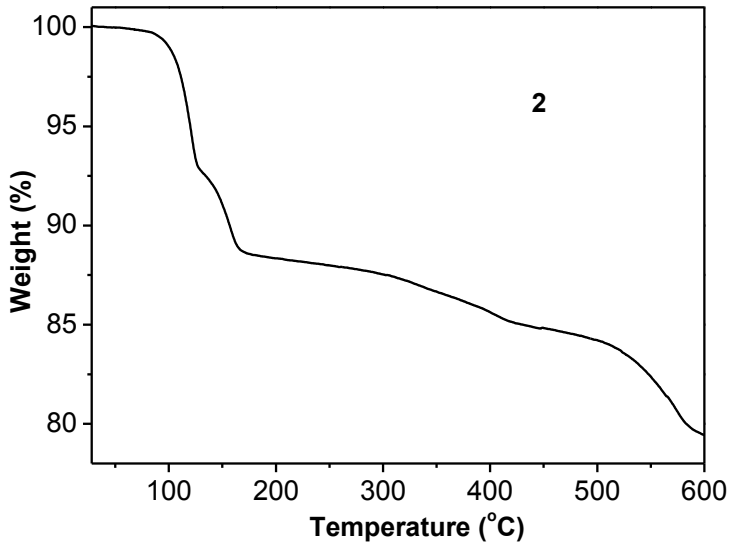

Fig. S10 TG curve of compound **2**.

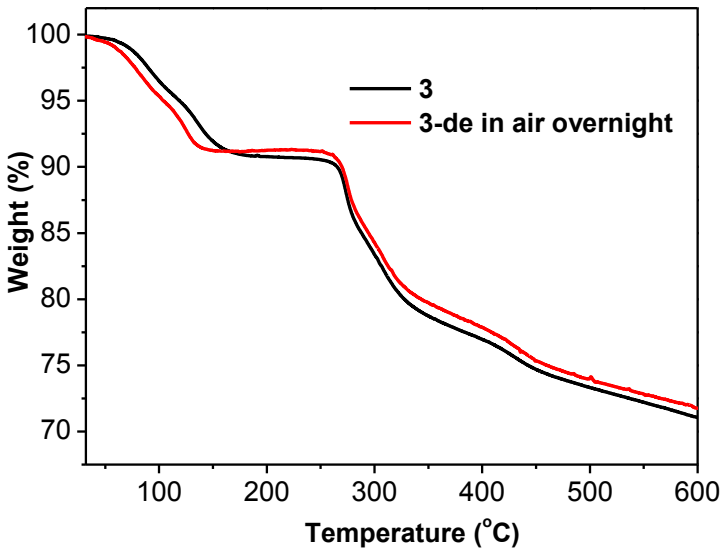

Fig. S11 TG curve of compound **3** and **3-de** in air overnight.

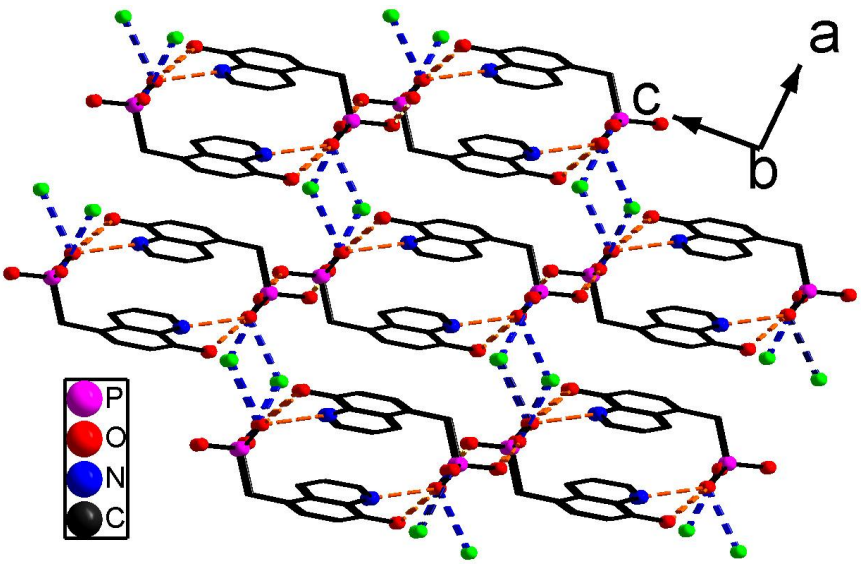

Fig. S12 The supramolecular three-dimensional structure of **1**·H_2O.

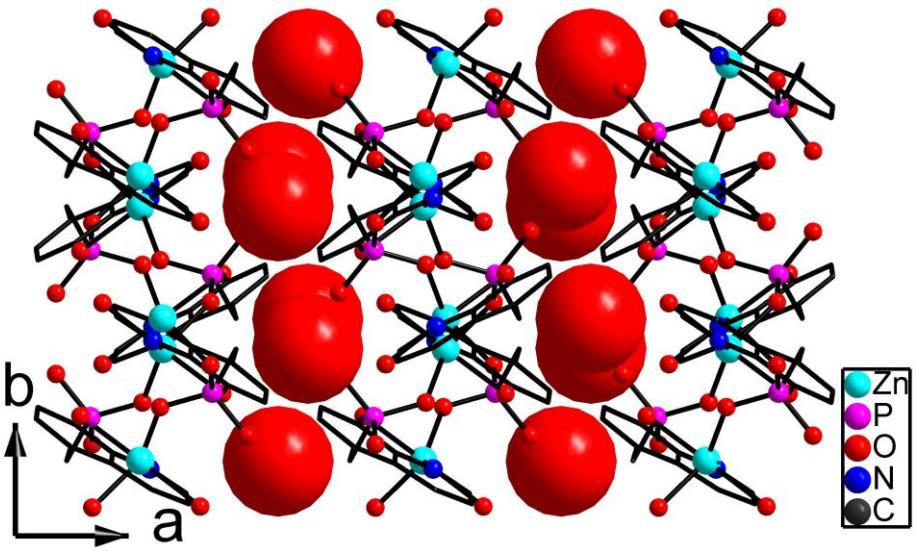

Fig. S13 The supramolecular three-dimensional structure of **2**.

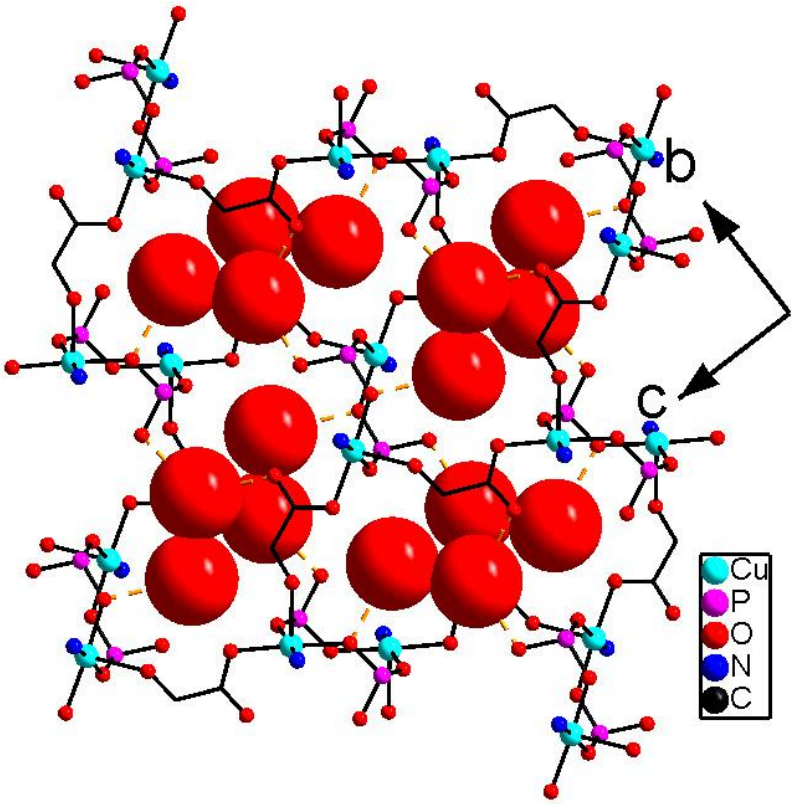

Fig. S14 The hybrid layer containing lattice water molecules in **3**.

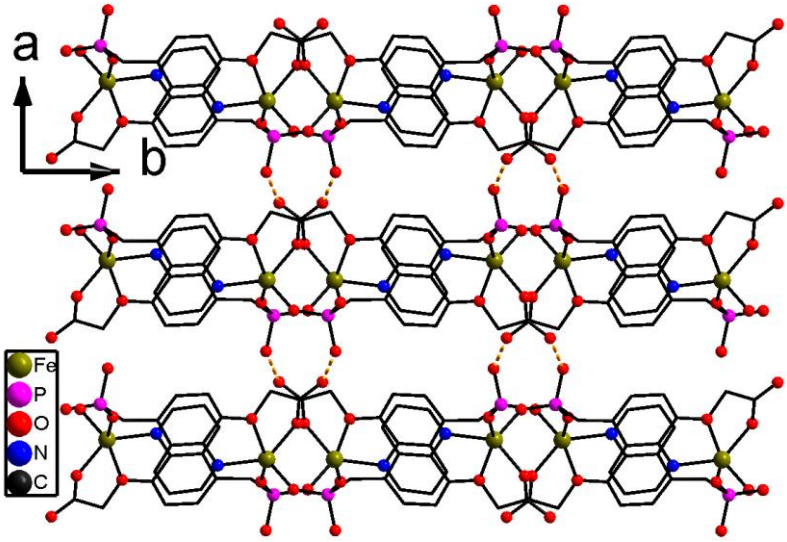

Fig. S15 The supramolecular three dimensional structure of **4**.

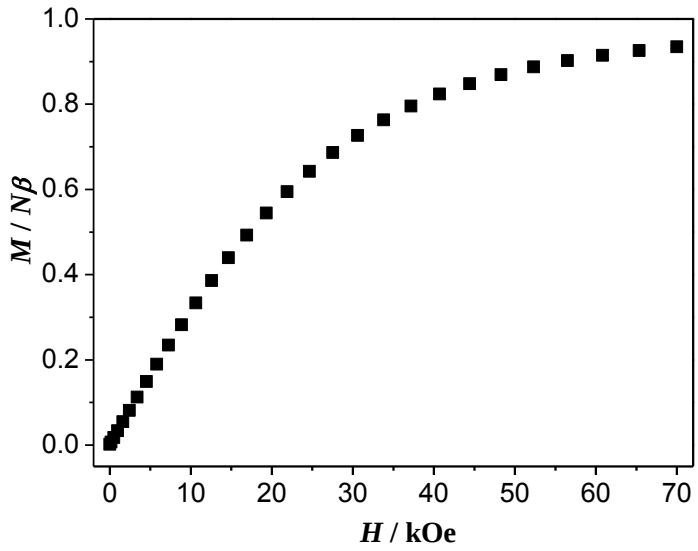

Fig. S16 Field-dependent magnetization for **3** at 1.8 K.

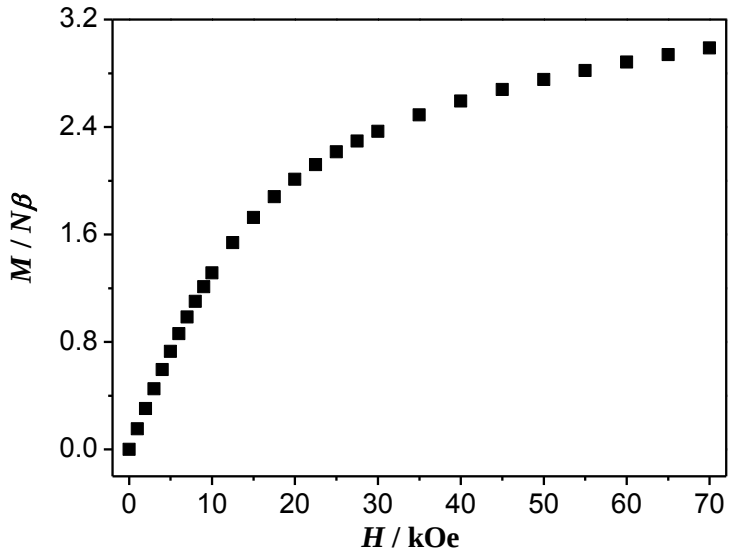

Fig. S17 Field-dependent magnetization for **4** at 1.8 K.